Soft Matter

PAPER

View Article Online
View Journal | View Issue

Cite this: *Soft Matter*, 2014, **10**, 5763

Phase segregation of sulfonate groups in Nafion interface lamellae, quantified *via* neutron reflectometry fitting techniques for multi-layered structures†

Steven C. DeCaluwe,[ab] Paul A. Kienzle,[b] Pavan Bhargava,[bc] Andrew M. Baker[bd] and Joseph A. Dura*[b]

Neutron reflectometry analysis methods for under-determined, multi-layered structures are developed and used to determine the composition depth profile in cases where the structure is not known *a priori*. These methods, including statistical methods, sophisticated fitting routines, and coupling multiple data sets, are applied to hydrated and dehydrated Nafion nano-scaled films with thicknesses comparable to those found coating electrode particles in fuel cell catalyst layers. These results confirm the lamellar structure previously observed on hydrophilic substrates, and demonstrate that for hydrated films they can accurately be described as layers rich in both water and sulfonate groups alternating with water-poor layers containing an excess of fluorocarbon groups. The thickness of these layers increases slightly and the amplitude of the water volume fraction oscillation exponentially decreases away from the hydrophilic interface. For dehydrated films, the composition oscillations die out more rapidly. The Nafion–SiO_2 substrate interface contains a partial monolayer of sulfonate groups bonded to the substrate and a large excess of water compared to that expected by the water-to-sulfonate ratio, λ, observed throughout the rest of the film. Films that were made thin enough to truncate this lamellar region showed a depth profile nearly identical to thicker films, indicating that there are no confinement or surface effects altering the structure. Comparing the SLD profile measured for films dried at 60 °C to modeled composition profiles derived by removing water from the hydrated lamellae suggests incomplete re-mixing of the polymer groups upon dehydration, indicated limited polymer mobility in these Nafion thin films.

Received 18th April 2014
Accepted 11th June 2014

DOI: 10.1039/c4sm00850b

www.rsc.org/softmatter

Introduction

Thin films play a vital role in a diverse array of advanced technologies, including electronics, magnetic data storage, batteries, fuel cells, pharmaceutical research efforts, and genetic sequencing devices. Such technologies benefit greatly from detailed structural information regarding the thin films involved. Reflectometry (using either neutron or X-ray probes) provides this structural characterization in the form of a depth profile of the scattering length density (SLD), a property of materials that can be determined from their composition and density. The technique measures the intensity of a reflected beam as a function of the grazing incident angle θ, often expressed as momentum transfer, Q. Neutron Reflectometry (NR) is widely used and has been successfully applied to the study of thin-film structures in polymers,[1–5] magnetic materials,[6–8] biological membranes,[9–16] and recently to the study lithium battery electrodes,[17,18] to name a few examples. NR can provide sub-Ångström precision for the thickness of layers typically greater than approximately 1.5 nm,[19–21] is sensitive to lighter elements than X-ray reflectometry and, given the isotope sensitivity of neutrons for many elements (including Li and H), can provide specific depth profiles of their concentration or can identify sources or processes that incorporate these elements into the thin films. Furthermore, neutrons are non-perturbing and can transmit with little attenuation through many solids, making NR particularly advantageous for *in situ* measurement of samples in non-ambient sample environments.[1,2,16–18,22,23]

Despite its many advantages, NR data can at times be difficult to analyze quantitatively. Similar to diffraction experiments,

[a]*Department of Mechanical Engineering, Colorado School of Mines, Golden, CO 80401, USA*

[b]*NIST-Center for Neutron Research, Gaithersburg, MD, 20899, USA. E-mail: joseph.dura@nist.gov*

[c]*Department of Electrical Engineering, University of Maryland, College Park, MD, 20742, USA*

[d]*Department of Mechanical Engineering, University of Delaware, Newark, DE, 19711, USA*

† Electronic supplementary information (ESI) available. See DOI: 10.1039/c4sm00850b

phase information is not measured in a single NR measurement. Although it is possible to obtain the neutron wave phase and directly invert NR data in a mathematically rigorous manner for some measurements,[13,24–30] this is not generally possible, so NR data are typically fitted to model SLD profiles.[25] These models can be specified by any number of analytical or free-form expressions, but are typically expressed as a series of thin film layers, each with specified thickness, interface width, SLD, and absorption parameter, with the fitting parameters adjusted to minimize the χ^2 goodness-of-fit statistic. While this approach is mature, widely used, and convenient, obtaining a good fit to a single data set only proves that the NR data is consistent with the proposed SLD profile, but is not sufficient to rule out symmetry-related solutions that may fit the data equally well. In addition, correlations between fitting parameters can complicate uncertainty estimation for these parameters. This is particularly problematic for structures with many layers, where there are larger numbers of fitting parameters. While *a priori* knowledge of the intended structure is often useful to eliminate some symmetry related fits and limit the range of the fitting parameters, in some classes of samples this knowledge is unavailable. Finally, determining SLD profiles for multi-layered samples may be inherently impossible if the samples consist of many similar layers such that some layers do not produce unique features in the data.

We describe here the analysis of NR data for samples with an unknown number of spontaneously formed layers, where there is no *a priori* information about either the composition of layers or the multilayer structure. Such structures are common in NR measurements, such as those involving chemical[31] and electrochemical[17] surface reactions and the spontaneous ordering of polymers.[1,32,33] The methods described here are used to fit NR data from multi-lamellar interfacial water structures in Nafion[34] thin films deposited on SiO_2 substrates, as described previously,[1] in order to elucidate what can be determined about the lamellar structures, how accurately we can know these structures, and what this indicates about phase-segregation in Nafion thin films. Nafion is composed of hydrophobic, PTFE-like backbone fluorocarbon chains and hydrophilic, sulfonic-acid terminated fluoro-ether side-chains. These two phases are known to segregate when Nafion is hydrated, with hydrated sulfonic acid side-chains forming nano-phase domains in a PTFE-like polymer matrix. The exact structure of these phases is still debated in the literature, including interconnected networks of inverted micelle clusters,[35] cylinders with either polymer[36] or water[37] in the center, branched cylindrical domains[38,39] and bundles of parallel cylindrical water clusters.[40] It has been established that the phase-segregation takes a multi-lamellar form at the interface between Nafion and SiO_2, while a single water-rich layer exists at Nafion's interface with metals such as Pt and Au.[1]

Such structures can have important implications for transport,[41] kinetics, and degradation pathways in polymer electrolyte membrane fuel cells (PEMFCs), particularly near hydrophilic additive particles[42] or in the catalyst layer, where thin layers of Nafion ionomer (1 to 100 nm, typically[43,44]) coat catalyst particles and carbon supports. The properties of the ionomer here are significantly influenced by the interfaces with the catalyst, support, and vapor phases, and can deviate significantly from bulk Nafion properties. By studying films in a similar thickness range (5 to 50 nm), this study probes the nature of Nafion hydration and lamellar phase segregation in dimensionally-confined layers to determine the structure of the lamellae and the total number of lamellae present.

Two films with equivalent Nafion thicknesses 42 nm (sample t42) and 5 nm (sample t5), are reported. For t42 we apply two approaches, Bayesian statistics and a damped oscillator model to determine the extent of the lamellar region, *i.e.* the number of interfacial lamellae that are distinct from the bulk-like morphology present further from the interface, in both highly hydrated and dehydrated states. Sample t5 was prepared with a thickness similar to that of the total lamellar region, in order to probe the potential influence of confinement and surface ordering on the decay of lamellar ordering away from the interface. Additionally, we take advantage of the simpler layered structure of this sample and isotopic contrast variation of the water to determine, in greater detail, the composition depth profile in the lamellar region at the level of Nafion components, *i.e.* the fluorocarbon chains and the sulfonic acid groups. Finally, a comparison of the two results sheds light on the origins of the residual lamellar structure in the dehydrated sample. These investigations are part of a larger exploration of PEMFC ionomer hydration with varying film thickness, the subject of a forthcoming publication.

Results and discussion

Bayesian analysis: sample t42 – 42 nm equivalent Nafion thickness

NR data for sample t42 measured at two relative humidity (RH) values, 92% RH (humidified with H_2O) and 0% RH vapor after complete drying, are shown as the discrete points in Fig. 1. Unless otherwise noted, error bars for a given data point and reported uncertainties represent ±one standard deviation. The high-Q peak corresponding to the multi-lamellar water structure at the Nafion–SiO_2 interface is clearly observed at $Q \approx 2.0$

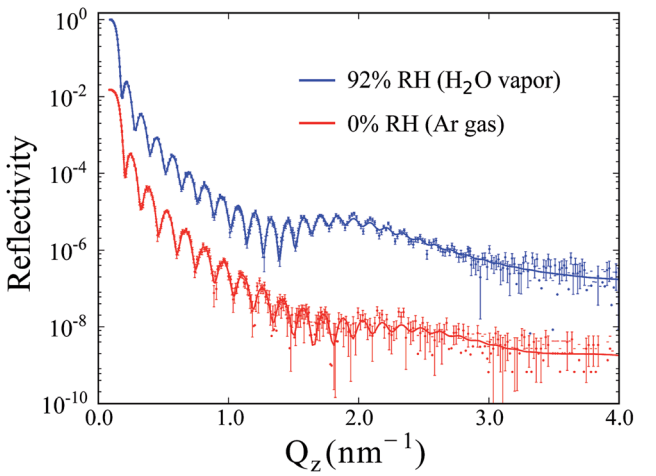

Fig. 1 NR data and best fits for moderately thin Nafion sample t42, as measured in 92% RH with H_2O vapor in Ar carrier gas, and 0% RH (dry Ar gas).

nm^{-1} for 92% RH. At 0% RH, the high-Q peak is still observable, but has shifted out to $Q \approx 2.3$ nm^{-1}, indicating a thinner structure, and has smaller amplitude, indicating a structure that has less SLD contrast with its surrounding layers (*i.e.* less water).

These data sets were fit independently using Refl1d[45] to models which included Si and SiO_2 substrate layers, a variable number of alternating water-rich and water-poor Nafion layers, followed by a thicker Nafion layer (where the phase segregation is 3-dimensional in nature, likely the same as in bulk Nafion membranes, and is averaged in the plane parallel to the substrate in specular reflectometry). Henceforth, the sheet-like phase-segregated layers at the Nafion–substrate interface are referred to as "the lamellae," while the term "layers" applies more generally to all sample layers (including substrate, native oxide, and bulk-like Nafion). The SLDs of the substrate and native oxide layers were held fixed at the known bulk values, while the thickness and surrounding interface widths of the native SiO_2 layer were fit. So that Refl1d could robustly sample the parameter space, the number of fitting parameters was reduced by using a common value for the interface widths between the lamellae, since the scattering is least sensitive to differences in those individual parameters. For this series of models, the "independent lamellae models," the SLDs and thicknesses of the individual lamellae were varied independently (another approach is discussed below). For the bulk-like Nafion layer, the SLD, thickness, and Nafion–vapor interface width were all fit. The SLD values of each Nafion-containing layer (lamellae and bulk-like layer) were modeled as a combination of the SLDs for water and dry Nafion ($SLD_{H_2O} = -0.56 \times 10^{-4}$ nm^{-2}, $SLD_{Nafion} = 4.16 \times 10^{-4}$ nm^{-2}):

$$SLD = SLD_{H_2O} V_{water} + SLD_{Nafion} V_{Nafion} \quad (1)$$

where V_j represents the volume fraction of species j. Requiring that the volume fractions sum to 1:

$$SLD = SLD_{H_2O}(1 - V_{Nafion}) + SLD_{Nafion} V_{Nafion} \quad (2)$$

allows V_{Nafion} to replace SLD as the fitting parameter for each of these layers.

The use of eqn (2) assumes that the density and composition of the dry Nafion ionomer are bulk-like in all layers, which may not be valid, particularly in the lamellae. To relax this assumption, V_{Nafion} is allowed to vary between 0 and 125%, which is non-physical but increases the SLD upper limit to 5.34×10^{-4} nm^{-2} to capture any potential variations in SLD_{Nafion}. The interpretation of $V_{Nafion} > 100\%$ is discussed in greater detail below, with regard to sample t5.

Fig. 2 shows the reduced χ^2 and Bayesian Information Criterion (BIC) values *vs.* the number of fitting parameters for the independent lamellae models as filled points. As described in the Experimental methods, for models with different numbers of fitting parameters, the BIC determines whether any changes in goodness-of-fit for an increased number of fitting parameters are statistically meaningful. The insets focus on the best of these models, and include the number of lamellae for each model on the upper x-axis. For fits to the 92% RH data, the χ^2 values decrease continuously up to 5 lamellae (20 parameters) and approach an approximately constant value after that. The corresponding BIC values have a minimum at 6 lamellae. The poorer fits for models with fewer than 4 lamellae (larger χ^2 values) are evident from comparisons of the fitted reflectivity to the data (shown in the ESI Fig. S2†), most notably due to decreasing amplitude of the high-Q lamellar peak with decreasing number of lamellae. Simulated NR data sets from models with 4 or more lamellae appear similar to one another, in accord with the small differences in χ^2 for these models.

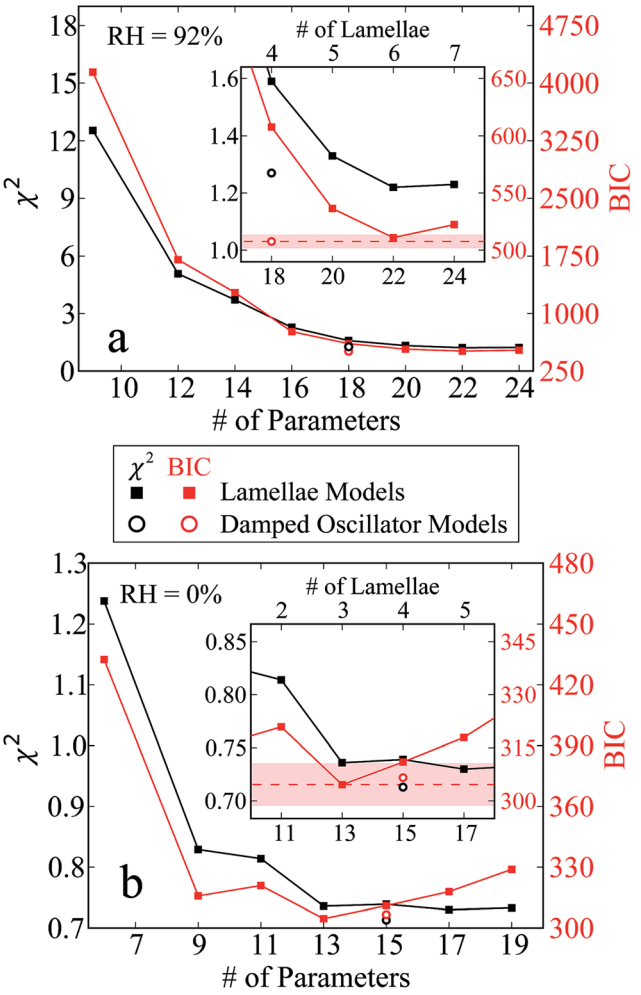

Fig. 2 Reduced χ^2 and BIC values for models with varying numbers of lamellae, fit to sample t42 for (a) data taken in 92 % RH; (b) data taken in 0% RH. Red shaded bands in the insets show the lowest BIC value ± 6, indicating the range of acceptable fits.

In the fits to the 92% RH data, the SiO_2 parameters were found to vary insignificantly with the number of lamellae and therefore the values from the best fit were adopted and held fixed when fitting the 0% RH data, giving these models 3 fewer fitting parameters. The 0% RH χ^2 values decrease rapidly with increasing number of lamellae through 3 lamellae, and much more slowly to 6 lamellae. The 3-lamellae model has the minimum BIC value. Simulated NR data from models with

fewer than 3 lamellae (Fig. S3†) show a poor match to the measured data in the region of the residual high-Q peak.

While χ^2 approaches a constant value and a minimum is observed in the BIC, it is possible that better fits (lower χ^2) exist for models with greater numbers of lamellae, but are not identified because the large number of parameters can make the global minimum in χ^2 difficult to locate. To test whether a greater number of lamellae could significantly improve the fits, a model was formulated to reduce the number of fitting parameters by sacrificing the ability to vary lamellae compositions and thicknesses independently. As described by Dura, *et al.*,[1] the lamellae begin with a water-rich lamella adjacent to the native SiO_2, after which Nafion-rich and water rich lamellae alternate with a composition amplitude that decreases toward a midrange water content in the bulk-like layer at the surface. This is similar to decaying composition modulations seen in block copolymers.[46] The lamellae's composition profile was thus modeled as a damped oscillator, with the composition of the lamellae decaying exponentially toward the bulk layer composition:

$$V_{\mathrm{Naf},m} = \begin{cases} V_{\mathrm{Naf,bulk}} - \Delta V_{\mathrm{w}}\, \mathrm{e}^{-m\,\sigma_{\mathrm{w}}} & \text{m is odd} \\ V_{\mathrm{Naf,bulk}} + \Delta V_{\mathrm{N}}\, \mathrm{e}^{-m\,\sigma_{\mathrm{N}}} & \text{m is even} \end{cases} \quad (3)$$

where $m = 1$ corresponds to the lamella adjacent to the native SiO_2, $V_{\mathrm{Naf,bulk}}$ is the fitted Nafion volume fraction of the bulk-like layer, ΔV_{k} is the maximum deviation from the bulk composition for each type of lamella (k = w for water-rich lamellae, k = N for Nafion-rich lamellae), and σ_{k} is the exponential rate of decay toward the bulk composition for each type of lamella. ΔV_{k} and σ_{k} values are constrained so that the volume fraction is between 0 and 125% for all lamellae, as was done for the independent lamellae models. The lamella thicknesses were modeled according to the following:

$$T_{\mathrm{m}} = \begin{cases} T_{\mathrm{w},0} \times {\gamma_{\mathrm{w}}}^{m} & \text{m is odd} \\ T_{\mathrm{N},0} \times {\gamma_{\mathrm{N}}}^{m} & \text{m is even} \end{cases} \quad (4)$$

where $T_{\mathrm{k},0}$ serves as a "baseline" thickness for the Nafion- or water-rich lamellae, and γ_{k} is a geometric rate of thickness change. (Note that other models for thickness change could be implemented with an equal number of parameters, such as a linear series $T_m = T_{\mathrm{k},0} + m \times \Delta T_{\mathrm{k}}$). As before, the SiO_2 parameters for fits to the 0% RH data were fixed at those from the best fit to the 92% RH data. Compared to the independent lamellae models, this "damped oscillator" (DO) model determines the lamellae SLD profile using 9 parameters – the same number of parameters used in the 4-lamellae model, above – but allows an arbitrary number of lamellae, with no additional 'penalty' in the BIC for additional lamellae. The number of lamellae is theoretically unlimited, although in practice the sum of the lamella thicknesses must be less than the total sample thickness. The DO model was run with 11 lamellae, which was found to be more than sufficient. The "correct" number of lamellae supported by the data is found by counting those with SLD values that differ significantly from that of the bulk-like outer Nafion layer. BIC and reduced χ^2 values for this fit are included in Fig. 2 with open symbols, which demonstrate an improvement the fit of the 92% RH data. While the χ^2 value for the DO model is higher, the small number of parameters reduces the BIC value (507.6) below that of the 6-lamellae model (510.9). The increased model complexity for the 6-lamellae model is therefore not justified by the minor improvement in χ^2 (1.22 *vs.* 1.27 for the DO model).

For the 0% RH data, the DO model does not improve the fit. The model with 3 independent lamellae remains better by a small factor (BIC = 304.6 *vs.* 306.6 for the DO model), despite a χ^2 value (0.74) that is marginally higher than for the DO model (χ^2 = 0.71). A BIC difference greater than 6 between two fits presents a "strong" case for rejecting the fit with the higher BIC.[47] The shaded bands in the Fig. 2 insets include the lowest BIC ± 6 for each data set; any BIC values within this band therefore represent fits that are statistically not strongly distinguishable from one another. For 92% RH, both the DO and 6-lamella models represent acceptable fits to the data. Similarly, the DO and 3-lamella models both give acceptable fits to the 0% RH data. The solid lines in Fig. 1 are the best fits from these models (3-lamellae model for 0% RH and the DO model for 92% RH) and show good agreement between the models and the data.

Although models were not fit simultaneously to the 92% and 0% RH data, post-fit material balance calculations demonstrate the remarkable consistency between the two best fits in the total amount of Nafion, represented here by the equivalent Nafion thickness, $t_{\mathrm{Naf}} = \sum t_i V_{\mathrm{Naf},i}$, summed over all i Nafion-containing layers. The t_{Naf} values were equal for the two RH conditions: t_{Naf} = 43.19[42.87, 43.40] nm for 92% RH and t_{Naf} = 42.43[42.16, 42.91] nm for 0% RH, affirming the accuracy of both the fit and the measurement technique. (Throughout this paper, numbers in brackets represent the 68% confidence intervals, the calculation of which are described elsewhere.[17,45])

The SLD profiles for the models deemed acceptable by the BIC analysis (as indicated in the Fig. 2 insets) are compiled in Fig. 3. Solid lines show the SLD profile for the best fit, while shaded regions show the 68% confidence intervals for each model, as described elsewhere.[17,45] Because SLD profiles have an arbitrary z-offset, they are shifted in z to co-align them on the center of the SiO_2 layer. Insets expand the lamellar region – note that the first high SLD layer, centered at $z = 0$ nm, corresponds to the native SiO_2 (SLD = 3.47×10^{-4} nm^{-2}). Despite the varying numbers of lamellae modeled, the SLD profiles are remarkably similar. The major exception is the best fit for the 6 lamellae model, which includes high interfacial widths on either side of the native SiO_2 layer and lower interfacial widths between the lamellae, compared to both the confidence interval bands for both models and to the DO model best fit. It is highly unlikely that the inter-lamellar interfacial widths will be lower than the SiO_2 interfacial widths (particularly the very smooth surface of the SiO_2, verified by numerous prior NR measurements). The similarity in the χ^2 values for the two best fits – despite quite different interfacial widths – demonstrates the limited sensitivity of NR to which width is assigned to which interface. This validates the use of a common interface width for all the lamellae, as discussed prior. The interfacial widths of the 6 lamellae model best fit are therefore presumed to be

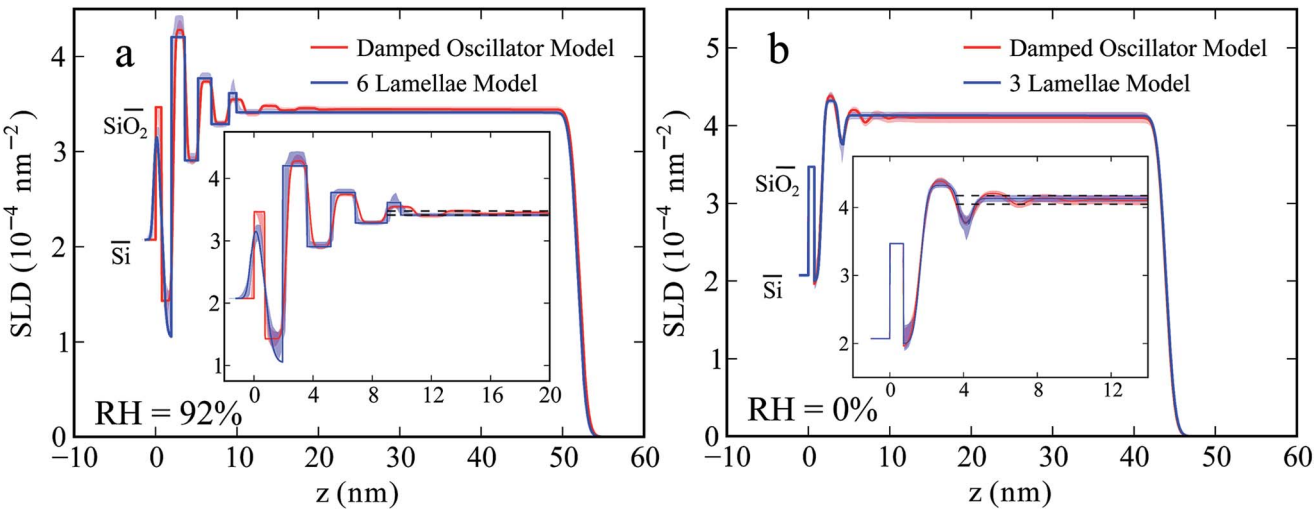

Fig. 3 SLD profiles for models with varying numbers of lamellae fit to sample t42. (a) 92% RH; (b) 0% RH. Solid lines show best fits and shaded regions show 68 % confidence intervals. Dashed lines in the inset are projections of the 68% confidence interval for the SLD of the bulk-like outer Nafion layer, which demonstrates that the 92% and 0% RH profiles have 6 and 3 lamellae, respectively, that are distinct from the bulk-like layer.

anomalous, and those given by the 68% confidence intervals and the DO model best fit are assumed to accurately depict the SLD profile. The narrow confidence intervals and close agreement between the various models in Fig. 3 demonstrate that the lamellae thicknesses and compositions are determined with high precision. Together these facts add confidence that within the context of lamellar models of the SLD profile, the envelope given by the combined 68% uncertainty for the various models accurately describes the lamellar structure at the Nafion–SiO_2 interface.

The dashed lines in the Fig. 3 insets represent the 68% confidence interval of the bulk-like outer layer SLD for each DO model fit, allowing direct comparison to the lamellae SLDs. At 92% RH, the DO model shows 6 lamellae with SLDs that are distinct from the bulk Nafion layer (*i.e.* those for which the 68% confidence interval of the lamella SLD has no overlap with that of the bulk-like Nafion SLD $[3.41, 3.48] \times 10^{-4}$ nm^{-2}, which corresponds to 14–16% water by volume). At 0% RH, the DO model shows roughly 3 lamellae with SLDs that vary significantly (as described above) from the bulk layer (SLD = $[4.06, 4.18] \times 10^{-4}$ nm^{-2}). The number of distinct lamellae in the profiles agree with the BIC analysis of the independent lamellae models in Fig. 2, lending further support that the 6 and 3 lamella models accurately describe sample t42 at RH = 92% and after drying. As shown in Fig. 4 and S5,† the lamellae get thicker

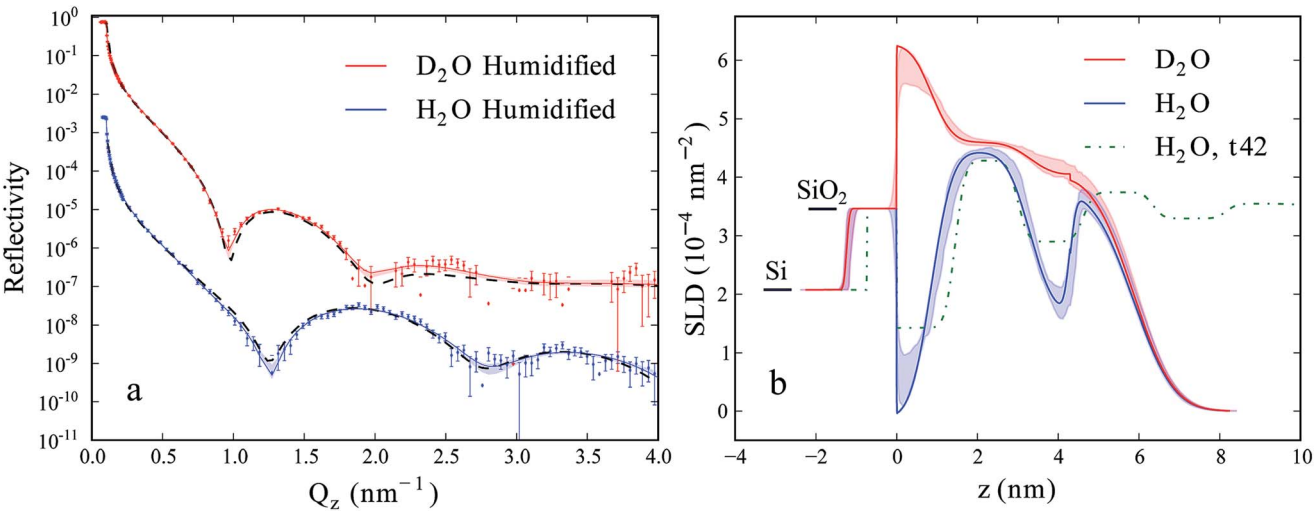

Fig. 4 Simultaneous fitting for ultra-thin Nafion sample t5, measured in Ar gas humidified to 92% RH by H_2O or D_2O. (a) NR data is shown by data points, with simulated NR from fitted SLD profiles overlaid. Black dashed lines show the simulated NR from the atomistic physical model given by the solid line in Fig. 6a. (b) Fitted SLD profiles, with t42 lamellar SLD profile (green dashed line) overlaid for reference. For both figures, solid lines show best fits while shaded regions show 68% confidence intervals.

as the lamellar order relaxes toward bulk nanophase structure away from the interface.

Simultaneous fitting: sample t5 – 5 nm equivalent Nafion thickness

Having determined the extent of the lamellar region, the Nafion thickness for the second sample was chosen to be less than this thickness and therefore truncate the lamellar region, in order to investigate if the lamellae are altered by proximity to the surface and to provide greater sensitivity to the lamellar structure in order to more accurately determine the molecular phase-segregation in this region. The NR for t5 was taken in 92% RH in both H_2O and D_2O vapor (the blue and red data points in Fig. 4a) for two advantages. Doing so provides an additional constraint to allow an independent determination of the water depth profile independent of any assumptions about the remaining material. This approach also differentiates between various symmetry-related SLD profiles[48] (see the ESI† for examples) by requiring a model that fits both the H_2O and D_2O measurements. The two data sets were fit simultaneously in Refl1d, using the same model as for sample t42, with up to 6 lamellae and an optional bulk-like Nafion layer. Substrate-related parameters were set to be equal between the two models, as were the thicknesses and interfacial widths of the Nafion layers.

Simultaneous fits which set the Nafion SLD equal to the bulk value ($SLD_{Nafion} = 4.16 \times 10^{-4}$ nm^{-2}) and employed SLD constraints to enforce equal water sorption from H_2O- and D_2O-humidified vapor did not return suitable goodness of fit, yielding summed χ^2 values > 14. Subsequent fits allowed each lamella's SLD for fits to D_2O and H_2O data to vary independently of one another, but retained lamellae thickness and interfacial width constraints. The data were best fit by a model with 4 lamellae with no bulk-like Nafion layer at the surface, as shown in Fig. 4b. The solid lines and shaded regions in Fig. 4a are the calculated NR for the best fits and the 68% confidence intervals, respectively, which show an excellent fit to the measured data, with a summed χ^2 value of 2.07. For reference, the best-fit SLD profile of the lamellar region of sample t42 is overlaid as a dashed green line in Fig. 4b. The thickness and SLD values of the lamellae are remarkably similar for these samples with fundamentally different total Nafion thicknesses. This indicates not only the lack of finite size effects on the lamellar structure but also the accuracy of the measurement, model, and best fits. The SLDs of the water-rich lamellae are slightly lower (more water) in the truncated sample, although the water-rich lamellae closest to the substrate are within the 95% confidence intervals of one another. The lower SLD of the third and fourth lamellae of the truncated sample is due to surface roughness.

Physical interpretation of the fitted SLD profiles can provide insight into the nature of phase segregation in Nafion near the SiO_2 interface. The poor fits obtained when the composition was constrained between the two models imply that either H_2O and D_2O are absorbed differently by the lamellae, or that the lamellae do not consist solely of water and bulk-like Nafion. Table 1 lists the V_{Nafion} values that correspond to the lamellae in each model in Fig. 4, according to eqn (2), with SLD_{Nafion} calculated according to the bulk density of dry Nafion. While a slight difference in absorption of the two water isotopes is possible or even likely,[49–51] it seems unlikely to explain the large differences in V_{Nafion} observed between the two models

Table 1 Nafion volume fractions (%), assuming lamellae consist solely of Nafion and water, and that samples absorb H_2O and D_2O equally. The significant differences between the two humidifying isotopes and the non-physical volume fractions (>100%) imply that the first assumption is invalid. Numbers in brackets represent 68% confidence intervals

	V_{Nafion} (%)	
Lamellae #	H_2O-humidified	D_2O-humidified
1	10.68 [10.68–37.71]	5.27 [0.0–43.64]
2	105.28 [101.27–108.01]	80.09 [76.82–86.82]
3	51.14 [41.96–59.09]	105.59 [79.55–112.77]
4	87.82 [82.18–96.19]	110.27 [87.27–116.82]

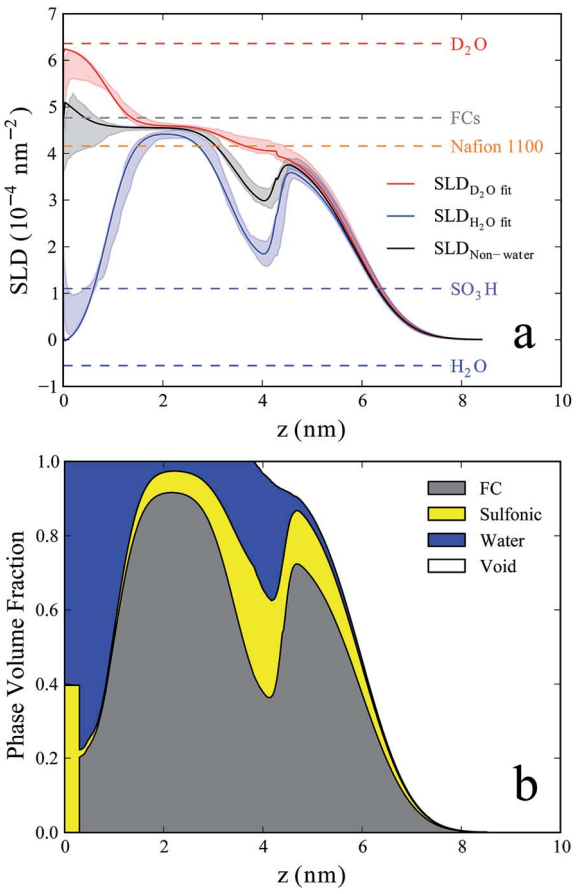

Fig. 5 Nafion composition depth profiles for sample t5. (a) Non-water SLD profile (black). SLD profiles for the fits to H_2O-(blue) and D_2O-humidified (red) films are shown for reference. Solid lines show best fits and shaded regions show 68% confidence intervals. Dashed lines show known SLDs for constituent molecular groups. (b) Volume-fraction depth profile for the physical model. Here, Nafion bonds to the SiO_2 substrate via the SO_3H side-chain terminal groups, with the side-chains stretched across the water-rich first lamella.

(Table 1), particularly given some of the non-physical volume fractions and the lack of a consistent relationship between $V_{\mathrm{Nafion,H_2O}}$ and $V_{\mathrm{Nafion,D_2O}}$. Furthermore, large differences in water absorption would also result in different lamellae thicknesses between the two models, which were not needed to obtain nearly ideal fits.

Instead, assuming equal uptake of H_2O and D_2O allows for analytical calculation of the water volume fraction depth profile and an independent determination of the material properties of the "non-water" phase. At a given depth z the fitted SLD in the H_2O and D_2O vapor data sets is assumed to consist of "water" and "non-water" portions, relaxing the assumption that the non-water portion is bulk-like dry Nafion:

$$\mathrm{SLD_{fit,k}}(z) = V_{\mathrm{water}}(z) \times \mathrm{SLD_{known,k}} + [1 - V_{\mathrm{water}}(z)] \times \mathrm{SLD_{non\text{-}water}}(z) \quad (5)$$

where $\mathrm{SLD_{fit,k}}(z)$ is the fitted SLD at depth z for humidifying vapor isotope k (k = H_2O or D_2O) and $\mathrm{SLD_{known,k}}$ is the known bulk SLD for the isotope k. Assuming that $V_{\mathrm{water}}(z)$ is the same for the H_2O- and D_2O-humidified samples gives the depth-dependent water volume fraction:

$$V_{\mathrm{water}}(z) = \frac{\mathrm{SLD_{fit,H_2O}}(z) - \mathrm{SLD_{fit,D_2O}}(z)}{\mathrm{SLD_{known,H_2O}} - \mathrm{SLD_{known,D_2O}}} \quad (6)$$

By substituting V_{water} from eqn (6) back into eqn (5) (for either isotope), one can also determine the SLD profile of the "non-water" portion.

The black line and shaded region in Fig. 5a show the SLD depth profile of the non-water portion of the material according to eqn (5) and (6) (the Si and SiO_2 layers are removed, for clarity). The fitted SLD profiles from Fig. 4b are included, for reference, along with horizontal dashed lines that indicate bulk SLD values for various constituent molecules, including H_2O and D_2O, the dry 1100 equivalent weight (EW) Nafion, and one way of partitioning Nafion into separate subcomponents: fluorocarbon groups (FC – the PTFE backbone, $(C_2F_4)_x$–C_2F_3, with x = 6.56 for 1100 EW Nafion, plus the non-sulfonic acid portion of the side-chain, $C_5F_{10}O_2$, which is mostly fluorocarbon, $\mathrm{SLD_{FC}} = 4.77 \times 10^{-4}$ nm^{-2}) and the sulfonic acid side-chain terminal groups (SO_3H, $\mathrm{SLD_{SO_3H}} = 1.1 \times 10^{-4}$ nm^{-2}). The non-water SLD profile consists of 4 distinct lamellae with different SLDs, none of which match that of bulk Nafion, indicating that the Nafion composition is different in each lamella. Three plausible interpretations for these SLD that differ from that of bulk Nafion are that the Nafion polymer (1) becomes less dense, characterized by incorporating un-filled pores/void space, (2) has increased density due to crystallization, and (3) breaks down into its constituent components, which segregate differently in the separate lamellae.

We next describe a model to interpret the SLD profiles from the simultaneous fit as a composition depth profile for the ultra-thin Nafion sample. Relating the non-water SLD profile in Fig. 5a to a composition profile represents an under-determined set of equations. In order to close the system of equations, the non-water SLD must consist of no more than two phases with known SLDs at any given depth. The non-water phase can, in general, be divided into three components: the fluorocarbon chains and sulfonic acid groups that make up Nafion, and vapor phase (SLD $\approx$ 0) encroaching due to surface roughness. For the two lamellae adjacent to the SiO_2, where the non-water SLD is greater than that of Nafion 1100, it is assumed that there is no vapor since that would further decrease the non-water SLD below the value for Nafion 1100 rather than raise it to the determined values. In the two lamellae adjacent to the vapor interface, the non-water SLD is less than that of Nafion 1100, and the vapor phase must be included. The simplest assumption to reduce the number of phases in these lamellae would be that the other component is a combination of fluorocarbon chains and sulfonate groups in the stoichiometric ratio for Nafion 1100. However, as shown in the supplementary information, this overall approach leads to deficit of sulfonate groups for the first two lamellae and therefore for the sample as a whole. While the global stoichiometry of the polymer can be satisfied by adding SO_3H groups to lamellae 3 and 4, adding them to lamella 4 deviates from the likely conformation of the Nafion polymer, given that the side chains are roughly 1 nm in length and the associated FC groups in lamellae 1 and 2 are located an average of 1.7 nm and 3.4 nm from lamella 4, respectively. While lamella 3 lies at nearly the correct distance from layers 1 and 2, the stoichiometry cannot be satisfied by adding SO_3H groups to lamella 3 alone.

In order to create a model that preserves the overall and local Nafion stoichiometry, an atomistic "physical model" based on Fig. 5a and on current knowledge of Nafion phase segregation is proposed. Model parameters are adjusted to be consistent with the multi-contrast NR data in Fig. 4. The simple approach described in the previous paragraph is modified in two ways; sulfonate groups are added at the Nafion/native oxide interface and in lamella 3 to satisfy the Nafion stoichiometry.

It is believed that Nafion is bonded to the SiO_2, based upon the fact that before annealing, Nafion spin coated onto SiO_2 will readily dissolve in water, whereas annealing the film prevents dissolution.[1,52] This bonding is presumably by an interaction between the sulfonic acid and the SiO_2.[52–54] Because of the large deficit of SO_3H groups in the water-rich lamella 1, the physical model thus assumes that the FC groups in this lamella consist entirely of side-chains (*i.e.* the hydrophobic backbone molecules are excluded from the lamella), which stretch across the lamella and bind the polymer to the substrate, terminating with SO_3H groups at the SiO_2 interface, with the remaining volume filled with water. The volume of SO_3H groups for this distinct interface layer is determined from the volume of the FC in lamella 1. In order to preserve the total sample thickness to remain consistent with the NR data, the thicknesses of the surrounding layers (native SiO_2 and water-rich 1st lamellae) must be reduced when adding this interfacial layer to the model. Any thickness removed from lamella 1 reduces the side-chain volume, which in turn reduces the volume of SO_3H groups in the partial monolayer at the SiO_2 interface. For a given number of SO_3H groups, the actual thickness of this interfacial layer will determine its composition (the ratio of SO_3H to water), and therefore its SLD. As described below, the thicknesses for

Table 2 Summary of assumptions used in the atomistic physical model. "Interface" layer refers to the SO_3H + water monolayer added at the substrate/Nafion interface for this model

Layer	Non-water SLD	Porosity	V_{FC} and V_{SO_3H}
Interface	Not calculated	0	$V_{FC} = 0$. V_{SO_3H} calculated to preserve Nafion 1100 stoichiometry under the assumption that layer 1 FCs are side chains. Remainder is H_2O
1	Center of 68% Cl in Fig. 5a	0	Calculated from $SLD_{non\text{-}water}$, assuming porosity = 0
2	Best fit from Fig. 5a	0	Calculated from $SLD_{non\text{-}water}$, assuming porosity = 0
3	Best fit from Fig. 5a	$1 - V_{water} - V_{FC} - V_{SO_3H}$	Assumes that the polymer has the composition of Nafion 1100, plus SO_3H groups needed to preserve Nafion 1100 stoichiometry of the overall sample
4	Best fit from Fig. 5a	$1 - SLD_{non\text{-}water}/SLD_{Nafion}$	Assumes that the polymer has the composition of Nafion 1100

the native oxide, interfacial SO_3H, and water-rich 1st lamella for the physical model were fit to the NR data, resulting in an interfacial layer that is 0.3 nm thick composed of 39.7% SO_3H and 60.3% water by volume (Fig. 5b) with 0.18 nm of the thickness subtracted from lamella 1 and the remaining 0.12 nm subtracted from the SiO_2. This thickness and volume fraction of SO_3H corresponds to a partial monolayer with an effective thickness of 0.12 nm (or 10.5 ng cm^{-2}).

The FC volume of lamella 2 is then modeled as a combination of polymer backbones corresponding to the side-chains from lamella 1, plus additional backbones and side-chains in the standard ratio for Nafion 1100. Based on the total FC content of lamellae 1 and 2, SO_3H groups are added to lamella 3 to satisfy the total stoichiometry of lamellae 1 through 3. The resulting composition profile is shown in Fig. 5b, and for clarity the assumptions used to calculate the composition of each lamella are summarized in Table 2. In this profile, the SO_3H groups in lamella 3 are distributed in such a way as to minimize discontinuities in the SO_3H and the vapor volume fractions at the interface between lamellae 3 and 4. The vapor exists only in the near-surface region and can here be interpreted as the result of surface roughness.

The profile in Fig. 5b therefore preserves overall Nafion stoichiometry and is consistent with the known lengths and hydrophilic interactions of the Nafion constituents (FC and SO_3H groups). The distribution of FC and SO_3H groups between lamellae determined by the model assumptions turns out to also be qualitatively consistent with the water content of each lamella, *i.e.* water-poor lamellae have an excess of FC groups (which are dominated by the hydrophobic PTFE backbone), and the water-rich lamellae have an excess of the hydrophilic SO_3H groups. Quantitatively, the λ values – the moles of water per mole of SO_3H – for lamellae 1 to 4 are, respectively, 34.6, 7.1, 5.4, and 1.5. Because the polymer morphology varies between the lamellae, and because of uncertainties in the determined composition, the slight variations in λ for lamellae 2 and 3 appear reasonable, but it is noteworthy that λ in lamellae 1 is considerably larger than for the other lamellae. The actual solvation of the SO_3H bonded to the substrate may be reduced by the presence of the substrate, which blocks access of the water molecules to the SO_3H, but is still likely higher than for lamellae 2 through 4. One likely explanation is that the hydrophilic SiO_2 substrate surface attracts additional water to this interface. Previous measurements have observed water-rich layers attracted to the polymer–SiO_2 interface for several other systems which do not display the lamellar structure observed here for Nafion.[55,56] While lamellar phase segregation is therefore not necessary for such water-rich layers, the water volume fraction observed for lamella 1 in this study (78%) is much higher than in these previous studies (17–30%), indicating that

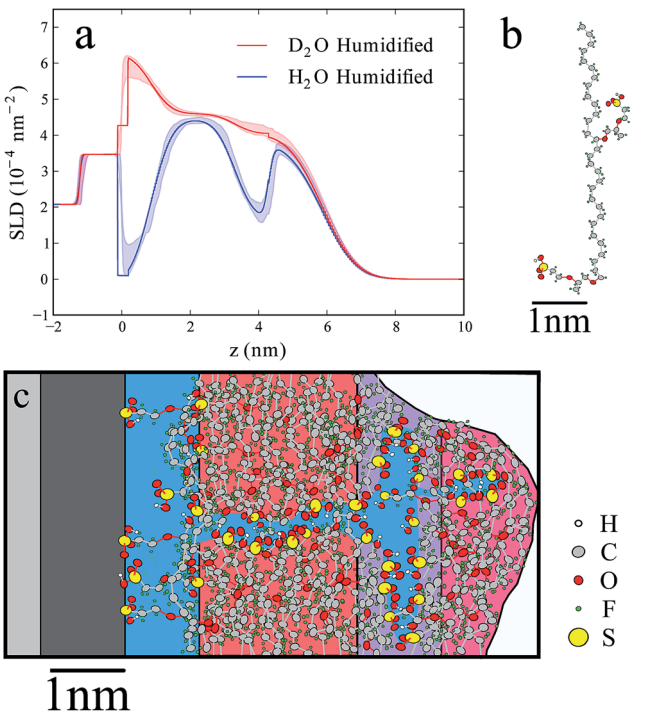

Fig. 6 Proposed atomistic physical model, based on composition depth-profile in Fig. 5b. (a) SLD profiles for a partial fit to the physical model (solid lines), compared to 68% confidence intervals for fits to H_2O- and D_2O-humidified vapor from Fig. 5a (shaded regions). (b) Nafion 1100 repeat unit, including both folded and un-folded side-chain morphologies. (c) Illustration of physical model.

the SiO_2 substrate and the polymer phase segregation likely both influence the high water content observed here. This additional water at the interface may explain how the substrate hydrophilicity induces the lamellae, which are absent or less prominent on substrates more hydrophobic than SiO_2 (as seen in ref. 1, 55 and 57 and in unpublished measurements taken at NIST where HF is used to remove the SiO_2 from the substrate). Another possible explanation for the high λ value in lamellae 1 is that the sulfonic acid at the substrate interface is more isolated from the FC backbone and can be more highly solvated with a reduced energy cost for swelling the polymer. For the water-poor lamella 4, it is unclear whether the low λ value is a physical phenomenon, due to factors such as the hydrophobic layer known to segregate to the Nafion surface in vapor environments,[58,59] or whether it is simply an artifact of the assumptions used to close the system of equations.

To explore the consistency of the physical model with the NR data, a model with the composition profile shown in Fig. 5b was constructed and the calculated NR was compared to the data. Minimal fitting was performed: only the thickness of the interfacial layer and how much of this thickness was subtracted from each of the adjacent layers (*i.e.* the SiO_2 substrate and water-rich first lamella) were varied. During fitting, the composition of the interfacial layer was calculated as a function of the thickness of the first lamellae, to maintain the stoichiometry between the SO_3H volume of this layer and the side-chain volume in lamella 1, as described above. The resulting SLD profiles (for H_2O and D_2O vapor data) are shown as solid lines in Fig. 6a. The 68% confidence intervals of the fitted SLD profiles from Fig. 4b are overlaid for reference. The simulated NR data based on the fitted physical model are shown as black dashed lines in Fig. 4a. These limited fits resulted in a summed χ^2 value of 3.40. While this is greater than that for the fits shown in Fig. 4 (summed $\chi^2 = 2.07$), it is low enough to imply that the model is consistent with the NR measurements, particularly considering that there were only two fitted parameters. Although a full re-fitting with this model would reduce the summed χ^2 further, the detailed element conservation employed herein would increase the model complexity significantly, and is beyond the scope of this work.

An illustration of the Nafion 1100 repeat unit, based qualitatively on previous atomistic simulations,[60,61] is shown in Fig. 6b; this repeat unit is used in an illustration of the proposed physical model shown in Fig. 6c. The illustration demonstrates that the proposed bonding of SO_3H side-chain terminal groups to the SiO_2 substrate, with the side chains stretching across a water-rich first lamella, is consistent with the known molecular structure and length scales. Subsequent lamellae demonstrate the alternating phase segregation between water-rich and water-poor lamellae, with SO_3H groups lining the interfaces between these domains that is also consistent with this repeat unit, and a monotonic increase in pore volume fraction in the two near-surface lamellae due to surface roughness. This structure is qualitatively similar to DFT simulations by Kendrick, *et al.*,[54] and molecular dynamics simulation results by Borges, *et al.*[53] The proposed physical structure of the lamellae, where water-poor lamellae consist almost entirely of PTFE-like backbones with side chains that extend outward into the water-rich (ionic) domains, is also similar to the proposed structure and size of Nafion crystallites.[62] The formation of the lamellae may thus represent a form of Nafion crystallization, where crystallites orient in sheet-like lamellae aligned with the substrate surface.

While the model in Fig. 5b and 6c is thus consistent with the NR data, the thin inter-lamellae interfacial layers are below the resolution of the NR technique with the current sample cell. The intent of the physical model is to interpret the SLD profiles in Fig. 4b in a way that is simultaneously consistent with the NR data and with the phase-segregation and bonding of hydrated Nafion. It is important to reiterate that while this analysis of the non-water composition profile is a reasonable match to the data and the known Nafion properties, it cannot rule out other possible solutions. However, the fits to the data do provide an unambiguous calculation of the water profile with sub-nm resolution in thin-film multi-lamellar Nafion structures. The variations in the non-water SLD and the physically relevant interpretation of the Nafion composition profile presented here strongly suggest that the fluorocarbon and sulfonate groups segregate preferentially into the water-poor and water-rich lamellae, respectively, near the SiO_2 interface. Furthermore, the model indicates that these variations are in excess of those predicted by a constant λ.

The composition profile of dehydrated lamellae – comparing t42 and t5

In hydrated films, the detailed description of the segregation of the Nafion components in the various lamellae was obtained by simultaneously fitting data collected on sample t5 with two water isotopes. The dehydrated films also showed a "remnant" lamellar structure (t42 at RH = 0%, Fig. 3b). While it has been previously reported that the drying procedure used here fully removes the water from the non-lamellar portion of the film,[1] the composition variations associated with the lamellae in the dried film are not yet understood. Fits to the single measurement of a dried sample do not provide the same level of detail as the contrast variation

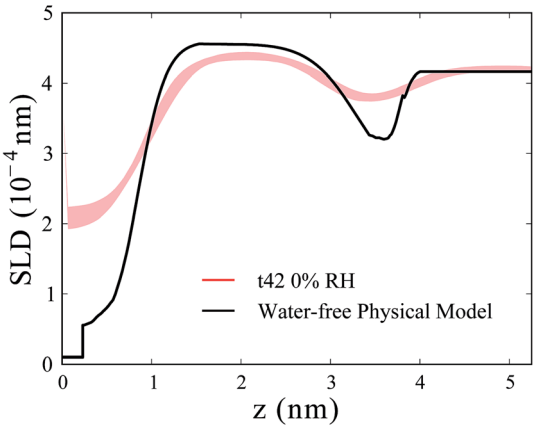

Fig. 7 SLD profiles of the lamellar region in dried Nafion thin films. Red shaded region – 68% confidence interval for the fit to sample t42 in 0% RH. Black line (water-free physical model) – the composition profile in Fig. 6c is converted to an equivalent SLD profile where all of the water is removed from layers not adjacent to the substrate.

afforded by humidifying in both D_2O and H_2O. To shed further light on the issue, the SLD profile of the dried t42 sample was compared to the SLD profile of the physical model of t5 (Fig. 5b) after removing some or all of the water but retaining the segregation of the Nafion component groups.

At each location z in the profile, the volume fractions of the solid portions (FC and SO_3H) are renormalized, after subtracting the water. Likewise, the distance Δz between adjacent profile locations is renormalized, according to the volume fraction of the water removed. The "water-free physical model" SLD profile is then calculated according to this reformulated composition profile, as the sum of the constituent SLDs weighted by their re-normalized volume fractions. The amount of water to remove from each lamella was determined by matching the renormalized lamella thickness with the corresponding lamellae thickness in sample t42 (Fig. 3b).

The resulting water-free physical model SLD profile is shown as the black line in Fig. 7, overlaid on 68% confidence interval for the lamellar SLD profile of sample t42 at 0% RH. A remarkable thickness match was obtained when all water was removed from every lamella except for the one adjacent to the SiO_2 substrate, from which all water in the physical model was retained. When the water is removed from lamella 1 in sample t5, the thickness is roughly 5 times thinner than that in the dehydrated t42 profile. Due to the similar SLDs for vapor and H_2O, replacing the lamella 1 residual H_2O with void space, *i.e.* uncollapsed pores, or another form of low density Nafion would give an SLD profile roughly equal to that shown in Fig. 7. The first possibility, a water-rich lamella 1 (after dehydrating at 60 °C in flowing Ar for 2 hours) would suggest that the SiO_2 interface is sufficiently hydrophilic to retain the water, while the alternative explanation, unfilled pores, would perhaps suggest limited mobility/flexibility of the side-chains proposed in Fig. 6c to reside in lamella 1.

In addition to matching the lamellae thicknesses, the lamellae SLDs are also qualitatively similar for the two profiles in Fig. 7. Because the water-free physical model preserves the composition gradients observed at 92% RH, an exact match between the two SLD profiles would imply that the phase segregation of the polymer constituent groups does not relax at all upon dehydration. Rather than an exact match, the SLD oscillations in dehydrated sample t42 have lower amplitude than those in the water-free physical model. While a quantitative analysis is beyond the scope of this manuscript, inspection suggests that only a partial re-mixing of the nano-phase segregation of the sulfonic acid and fluorocarbon groups present in the water-free physical model is required to provide the best agreement between the two SLD profiles. Therefore, while the polymer phase segregation observed at RH = 92% does relax to some extent upon dehydration, results suggest that there is a considerable amount of phase segregation that is "locked in" to the sample, presumably due to low mobility of the polymer groups in the dehydrated films.

Conclusions

This study provides new insight into the nature of the multilamellar phase segregation in Nafion thin-films deposited onto SiO_2 substrates. In Nafion films that are thicker than the lamellar region, 6 lamellae form under high humidity, with compositions that are appreciably different from the bulk-like Nafion outer layer that forms more than 10 nm from the substrate. This structure can be described as a composition modulation with exponentially decaying amplitude. This is substantiated by the fact that the envelope of the SLD depth profiles given by the 68% uncertainty for the various models overlap (Fig. 3a), and therefore accurately describes the individual lamella thicknesses and compositions (regardless of whether or not the model explicitly includes the decaying amplitude). For Nafion films thinner than the roughly 10 nm lamellar region, the lamellar SLD profile under high humidity is remarkably similar to that for the thicker films (Fig. 4b), indicating that the structure is not influenced by surface or confinement effects. The structural differences in the thinner films can be fully explained by surface roughness. Upon dehydration, there are only 3 lamellae with a composition distinct from the bulk-like Nafion layer. Results suggest that these residual lamellae are largely due to a degree of persistent phase segregation of the polymer groups, (*i.e.* fluorocarbon and SO_3H) rather than water retained in the structure, implying low mobility for the polymer groups. The exception is for the lamella adjacent to the SiO_2 substrate, which either retains all of the water present at 92% RH, has a large volume fraction of unfilled pores (or low density Nafion), or some combination of the two.

The following physical model of the interfacial Nafion phase segregation formation is consistent with both the lamellar SLD profile and the known length scales and phase-segregation behavior of the Nafion repeat unit. Nafion is bonded to the SiO_2 substrate by interaction with the sulfonic groups. Water in excess of that associated with these of sulfonic acid groups is also present at the interface. The side-chains attached to these sulfonic acid groups extend across the water-rich first lamella. The second lamella contains fluorocarbon backbones associated with the sidechains in the first lamella, plus additional backbones and side-chains in the standard ratio for Nafion 1100. This lamella has fewer sulfonic groups than predicted by the equivalent weight, and is nearly devoid of water. In subsequent lamellae the Nafion sulfonic and fluorocarbon groups (backbone and side chain) segregate preferentially into the alternating water-rich and water-poor lamellae, respectively, with increasing intermixing away from the defining substrate. We speculate that, for these hydrophilic substrates, either the excess water at the hydrophilic interface or bonding of the sulfonic acid groups may be instrumental in establishing the lamellae (rather than other phase segregation morphologies), with a return to bulk-like morphologies away from this driving force.

The methods used in this study also make available a level of rigor for fitting reflectivity data taken on samples with spontaneously formed layers of undetermined number, composition, or structure. Statistical methods, sophisticated fitting routines, and coupling multiple data sets (either by simultaneous fitting or applying constraints such as conservation of mass) can greatly aid in model selection, definition, and evaluation, and in substantiating the information available from a given set of NR

data. Future reflectivity studies in which the structure or composition are not known *a priori* should greatly benefit from applying similar approaches, both to confirm that the proposed fits, as opposed to alternate models, are uniquely supported by the data and to demonstrate that the data is of the requisite quality and extent to support the purported structures.

Experimental methods

Fabrication of Nafion thin films

Nafion thin films were fabricated by spin-coating Nafion dispersions diluted in HPLC grade ethanol onto 5 mm thick polished single-crystal Si substrates. Such substrates provide a relatively smooth and warp-free surface, necessary for reflectometry measurements. Substrates were first cleaned with water and detergent then rinsed with Millipore deionized water. Water droplets were blown from the surface with N_2 gas, and then the substrates were exposed to UV–ozone for 30 minutes. The native oxide layer is thus left intact on the substrate surface. Substrates were then installed in a spin coater (Headway Research, Inc.), and rinsed with HPLC-grade ethanol and spun dry for 15 seconds to remove any residual water and/or surface contamination. Dispersions of Nafion resin (1100 equivalent weight, 20 wt% in solution of lower aliphatic alcohols and H_2O mixture; Sigma Aldrich) in HPLC-grade ethanol were pre-mixed to give a specified Nafion thickness. Dispersion-coated wafers were then spun at 3500 rpm (58.3 Hz) for 60 seconds and annealed under vacuum at 60 °C for 1 hour to bond the Nafion to the substrate and provide a consistent structure which, for Nafion, is highly dependent upon thermal history. In this study, two separate samples are measured with NR, referred to by their equivalent Nafion thickness (*i.e.* the thickness of the Nafion film if all water were removed): (i) a thicker sample, t42, with an equivalent Nafion thickness of approximately 42 nm, and (ii) a thinner sample, t5, with an equivalent Nafion thickness of approximately 5 nm.

Neutron reflectometry data collection

As stated, specular NR measures the reflected intensity as a function of grazing angle θ, or as a function of the momentum transfer $Q = (4\pi/\lambda_n) \times \sin\theta$, where λ_n is the wavelength of the neutrons (0.5001 ± 0.0004) nm for this study, measured after instrument realignment, and varying insignificantly from the value of (0.5006 ± 0.0003) nm reported in the literature.[63] Prior to measurement, samples were carefully aligned to achieve a surface that is parallel to ($\pm$0.0004 degrees) and bisecting ($\pm$0.01 mm) the incident, ribbon-shaped, beam. The beam profile is determined by four sets of vertical slits, two upstream of the sample and two downstream. For measurements in the range $0.5° < \theta < 6.5°$, the upstream slits were opened continuously at a rate of 0.4 mm per degree-θ, to provide a constant $\Delta Q/Q$, a flux that increases as Q^2, and a constant 4.3 cm wide beam projection onto the plane of the sample. Below this range, the upstream slits were held constant at 0.05 mm (t42 at 0% RH) or 0.1 mm (for all other measurements.) Above $\theta = 6.5°$ the incident slits are held fixed at 2.6 mm in order to keep the final slit from exceeding the detector limit. To reduce background the two downstream slits were maintained at 0.6 mm and 0.8 mm below $\theta = 0.5°$ and at 3$\times$ and 4$\times$ the width of the upstream slits, respectively, otherwise. An aperture just before the sample defined a roughly 25 mm beam width in the orthogonal direction.

The background signal was measured during two sets of scans with the slits and theta as in the specular scans, but with the detector offset slightly from the specular ($\theta \times 2$) condition, to $\theta \times 2.5$ and to $\theta \times 1.5$. These two background scans were averaged to provide an approximation of the background scattering at the specular condition. Small deviations from this linear interpolation between background measurements were modeled when fitting the data by a residual background fitting parameter that is invariant with Q. The reflected intensity is normalized by the incident intensity as a function of slit settings, which is measured in a separate scan with the beam also directed through the Al walls of the controlled RH sample environment (described below) to maintain the same beam attenuation as during specular and background scans. Specular data were taken as several repeated series of scans through the entire Q range of interest, to check for changes that might occur over time, particularly to ensure that the sample hydration had equilibrated. The specular reflectivity is determined by subtracting the averaged background scans from the specular scans and then normalizing by the incident intensity. The counting statistics of these individual measurements are propagated through the reduction to provide uncertainty estimates for the data at plus and minus one standard deviation.

Controlled RH sample environment

Because the water uptake of Nafion varies considerably with small variations in RH at high humidity, care was taken to maintain stable and reproducible control of the thermal environment and humidity. Samples were maintained at (29.6 ± 0.2) °C and (92.1 ± 1.5)% RH using a custom-built sample environment, shown schematically in Fig. S1.† Full details are given in the ESI section.† Samples are measured in up to three separate vapor atmospheres: (i) in H_2O-humidified Ar, (ii) in D_2O-humidified Ar, and (iii) at 0% RH in dry Ar carrier gas (with the dew point generator bypassed). Isotopic contrast variation between H_2O and D_2O allows for determination of the water concentration depth profile within the limits imposed by the isotopic variations in water uptake[49–51] and reproducibility of the RH, as discussed in the Results section. In order to remove any trace of H_2O or D_2O from the sample before beginning the next measurement, the sample was held at 60 °C inside the sample can under flowing dry Ar for at least 2 hours. The sample is never exposed to the ambient between measurements, and remains under controlled vapor composition and temperature between measurements. This procedure has previously been shown to remove all trace water from the non-lamellar portion of Nafion thin films, with only 1 to 2 water-rich lamellae remaining in the lamellae.[1] For exchanges between H_2O and D_2O, the dew point generator is drained entirely of the prior isotope and flushed 5 times with the new water isotope while the sample is dried.

Data fitting

The NR data is fit using the Refl1d[45] program, developed by NCNR and the University of Maryland as part of the DANSE project. Refl1d models the sample as a set of thin film layers with specified thickness and (real and imaginary) SLD, with specified Gaussian interface widths between them. Reflectivity is computed using the Abeles optical matrix method,[64] with interfacial effects computed by the method of Nevot and Croce.[65] Refl1d uses a DREAM algorithm[66] to generate a random collection of parameter sets from the entire parameter space. For each parameter set, the probability of observing the measured reflectivity is proportional to the likelihood $L = e^{-\chi^2/2}$. From this collection of parameter sets we can estimate the uncertainty in the individual parameter values and observe correlations between parameters. Because parameter correlations are preserved and explicitly incorporated into uncertainty estimates, error estimates *via* Refl1d are much more accurate than those given by standard gradient-descent methods. The DREAM algorithm is a population-based Markov Chain Monte Carlo method, which can effectively sample from low dimensional probability distributions with disjoint modes, and so unlike standard gradient-descent algorithms it operates as a reliable global optimizer.

For all fits, the SLDs of the substrate and native oxide layers were held fixed at the known bulk values, while the thickness and surrounding interface widths of the native SiO_2 layer were fit. For the bulk-like Nafion layer, the SLD, thickness, and Nafion–vapor interface width were all fit. Similar to the SLD values, the neutron absorption coefficients were modeled as a linear combination of the individual absorption coefficients, weighted by their volume fractions. Finally, each fit had 3 instrumental fitting parameters, corresponding to the small incident angle offset (within the motor tolerance), the residual background, and the incident beam intensity. In all, models had 10 fitting parameters plus 2 parameters for each lamella. Because of the large number of fitting parameters, the 92% and 0% RH data taken on sample t42 were not fit simultaneously. This would have limited value in that there are only 3 parameters common to the two models, corresponding to the SiO_2 thickness and both adjacent interface widths. Rather, the 92% RH data were fit first to a series of models with varying number of lamellae, $0 \leq n_{\text{lamellae}} \leq 7$. The SiO_2 parameters were found to vary insignificantly with the number of lamellae in the model. For fits to the 0% RH data, these parameters were therefore held fixed at the values obtained from the best fit to the 92% RH data. Fewer layers were needed to fit the 0% RH data, which was fit to models with up to 6 lamellae before χ^2 no longer improved.

Because the number of lamellae formed at the Nafion–SiO_2 interface is not known *a priori*, choosing the correct number of lamellae for the reflectivity model is non-trivial. As mentioned, the primary method for differentiating between NR models is by comparing the χ^2 value for each model. While increasing the number of lamellae may improve the χ^2 value for a particular sample, the decrease in χ^2 may simply be due to a better fit to the random statistical variations of the data (noise) rather than the systematic structure-induced variations. Therefore, for models with different numbers of lamellae (and therefore different numbers of fitting parameters) but similar χ^2 values, this study uses the Bayesian information criterion (BIC) to differentiate between models.[67] The BIC determines whether changes in goodness-of-fit are statistically meaningful by considering the expected improvement in likelihood due to the increased number of fitting parameters. This is achieved by maximizing a penalized log-likelihood function,[67] equivalent to minimizing the BIC:

$$\text{BIC} = (n - k)\chi^2 + k \ln(n) \quad (7)$$

where n is the total number of data points for the measurement, k is the total number of fitting parameters, and χ^2 represents the reduced chi-squared statistic.[68,69] All χ^2 reported herein represent the reduced χ^2.

In Refl1d, fitting parameters can be reformulated to represent composition or other relationships between parameters. Additionally, multiple data sets taken on a given sample (for example, exposed to different ambient conditions, *e.g.* humidified and dried) can be fit simultaneously. Advantages include enforcing common values for model parameters that do not vary between the two measurements, such as those associated with the substrate or impermeable buried layers, and eliminating erroneous models that provide suitable fits due to symmetry relations to the correct model (see ESI Fig. S6†). In this study, simultaneous fitting was used to fit the data for the thinner sample, t5. For this sample, the entire Nafion film consisted of the alternating water-rich and water-poor lamellae, and scattering from the lamellae and from the total sample thickness interacted in ways that made it difficult to distinguish between numerous models. The thinner sample was therefore measured in both H_2O- and D_2O-humidified vapor. Assuming equal uptake of H_2O and D_2O by the film, these data sets were fit simultaneously in Refl1d, as described above. In this manner, simultaneous fitting was able to differentiate between various symmetry-related SLD profiles[48] by requiring a model that fit both the H_2O and D_2O measurements.

Acknowledgements

The authors are grateful for the generous support of the National Academies' NRC Research Associateship Program (SCD), the NIST Summer Undergraduate Research Fellowship program (AMB and PB), and the NIST Summer High School Intern Program (PB). The DANSE project was funded by the US National Science Foundation under grant DMR-0520547.

References

1 J. A. Dura, *et al.*, Multilamellar Interface Structures in Nafion, *Macromolecules*, 2009, **42**(13), 4769–4774.
2 L. L. He, *et al.*, Interfacial Effects on Water Penetration into Ultrathin Ionomer Films: An in Situ Study Using Neutron Reflectometry, *Macromolecules*, 2009, **42**(15), 5745–5751.

3 R. Inoue, *et al.*, Interfacial properties of polystyrene thin films as revealed by neutron reflectivity, *Phys. Rev. E: Stat., Nonlinear, Soft Matter Phys.*, 2011, **84**(3), 031802.
4 E. Kharlampieva, *et al.*, Spin-Assisted Layer-by-Layer Assembly: Variation of Stratification as Studied with Neutron Reflectivity, *Langmuir*, 2009, **25**(24), 14017–14024.
5 E. Sivaniah, R. A. L. Jones and D. Higgins, Small Molecule Segregation at Polymer Interfaces, *Macromolecules*, 2009, **42**(22), 8844–8850.
6 M. R. Fitzsimmons, *et al.*, Influence of interfacial disorder and temperature on magnetization reversal in exchange-coupled bilayers, *Phys. Rev. B: Condens. Matter Mater. Phys.*, 2001, **64**(10), 104415.
7 M. R. Fitzsimmons and C. F. Majkrzak, *Modern Techniques for Characterizing Magnetic Materials*, ed. Y. Zhu, Kluwer Academic Publishers, Boston, 2005.
8 D. Niebieskikwiat, *et al.*, Nanoscale magnetic structure of ferromagnet/antiferromagnet manganite multilayers, *Phys. Rev. Lett.*, 2007, **99**(24), 247207.
9 D. A. Doshi, *et al.*, Neutron reflectivity study of lipid membranes assembled on ordered nanocomposite and nanoporous silica thin films, *Langmuir*, 2005, **21**(7), 2865–2870.
10 B. W. Koenig, *et al.*, Neutron reflectivity and atomic force microscopy studies of a lipid bilayer in water adsorbed to the surface of a silicon single crystal, *Langmuir*, 1996, **12**(5), 1343–1350.
11 S. Krueger, Neutron reflection from interfaces with biological and biomimetic materials, *Curr. Opin. Colloid Interface Sci.*, 2001, **6**(2), 111–117.
12 S. Krueger, *et al.*, Investigation of hybrid bilayer membranes with neutron reflectometry: Probing the interactions of melittin, *Langmuir*, 2001, **17**(2), 511–521.
13 C. F. Majkrzak, *et al.*, First-principles determination of hybrid bilayer membrane structure by phase-sensitive neutron reflectometry, *Biophys. J.*, 2000, **79**(6), 3330–3340.
14 C. F. Majkrzak, *et al.*, Structural Investigations of Membranes in Biology by Neutron Reflectometry, in *Neutron Scattering in Biology: Techniques and Applications*, ed. J. Fitter, T. Gutberlet and J. Katsaras, Springer Publishing, New York, 2006.
15 D. J. McGillivray, *et al.*, Structure of Functional *Staphylococcus aureus* alpha-Hemolysin Channels in Tethered Bilayer Lipid Membranes, *Biophys. J.*, 2009, **96**(4), 1547–1553.
16 C. W. Meuse, *et al.*, Hybrid bilayer membranes in air and water: Infrared spectroscopy and neutron reflectivity studies, *Biophys. J.*, 1998, **74**(3), 1388–1398.
17 J. E. Owejan, *et al.*, Solid Electrolyte Interphase in Li-Ion Batteries: Evolving Structures Measured In situ by Neutron Reflectometry, *Chem. Mater.*, 2012, **24**(11), 2133–2140.
18 H. Wang, *et al.*, *In Situ Neutron Techniques for Studying Lithium Ion Batteries, in Polymers for Energy Storage and Delivery: Polyelectrolytes for Batteries and Fuel Cells*, ed. C. Soles and J. Runt, Amer. Chem. Soc., 2012, pp. 91–106.
19 J. A. Dura, *et al.*, Neutron reflectometry, X-ray reflectometry, and spectroscopic ellipsometry characterization of thin SiO_2 on Si, *Appl. Phys. Lett.*, 1998, **73**(15), 2131–2133.
20 M. P. Seah, *et al.*, Critical review of the current status of thickness measurements for ultrathin SiO(2) on Si Part V. Results of a CCQM pilot study, *Surf. Interface Anal.*, 2004, **36**(9), 1269–1303.
21 M. P. Seah, *et al.*, Ultra-thin SiO_2 on Si IX: absolute measurements of the amount of silicon oxide as a thickness of SiO_2 on Si, *Surf. Interface Anal.*, 2009, **41**(5), 430–439.
22 M. Kreuzer, *et al.*, Pressure cell for investigations of solid-liquid interfaces by neutron reflectivity, *Rev. Sci. Instrum.*, 2011, **82**(2), 023902.
23 Q. Zhong, *et al.*, Switching kinetics of thin thermo-responsive hydrogel films of poly(monomethoxy-diethyleneglycol-acrylate) probed with in situ neutron reflectivity, *Soft Matter*, 2012, **8**(19), 5241–5249.
24 C. F. Majkrzak, *et al.*, Progress in the Development of Phase-Sensitive Neutron Reflectometry Methods, *Langmuir*, 2009, **25**(7), 4154–4161.
25 C. F. Majkrzak, N. F. Berk and U. A. Perez-Salas, Phase-sensitive neutron reflectometry, *Langmuir*, 2003, **19**(19), 7796–7810.
26 U. A. Perez-Salas, *et al.*, Characterization of a biomimetic polymeric lipid bilayer by phase sensitive neutron reflectometry, *Langmuir*, 2003, **19**(19), 7688–7694.
27 C. F. Majkrzak and N. F. Berk, Exact determination of the neutron reflection amplitude or phase, *Physica B*, 1996, **221**(1–4), 520–523.
28 C. F. Majkrzak, *et al.*, Phase determination and inversion in specular neutron reflectometry, *Physica B*, 1998, **248**, 338–342.
29 C. F. Majkrzak and N. F. Berk, Exact Determination Of The Phase In Neutron Reflectometry, *Phys. Rev. B: Condens. Matter Mater. Phys.*, 1995, **52**(15), 10827–10830.
30 C. F. Majkrzak and N. F. Berk, Exact determination of the phase in neutron reflectometry by variation of the surrounding media, *Phys. Rev. B: Condens. Matter Mater. Phys.*, 1998, **58**(23), 15416–15418.
31 P. A. Reynolds, *et al.*, Complex layering observed in high internal phase emulsions at a silicon surface by neutron reflectometry, *J. Colloid Interface Sci.*, 2011, **364**(2), 539–545.
32 J. W. Kiel, *et al.*, Nanoparticle concentration profile in polymer-based solar cells, *Soft Matter*, 2010, **6**(3), 641–646.
33 J. W. Kiel, *et al.*, Phase-sensitive neutron reflectometry measurements applied in the study of photovoltaic films, *J. Chem. Phys.*, 2010, **133**(7), 074902.
34 Certain commercial equipment, instruments, or materials are identified in this paper to foster understanding. Such identification does not imply recommendation or endorsement by the National Institute of Standards and Technology, nor does it imply that the materials or equipment identified are necessarily the best available for the purpose.
35 T. D. Gierke, G. E. Munn and F. C. Wilson, The Morphology In Nafion Perfluorinated Membrane Products, As Determined By Wide-angle And Small-angle X-ray Studies, *J. Polym. Sci., Part B: Polym. Phys.*, 1981, **19**(11), 1687–1704.
36 L. Rubatat, G. Gebel and O. Diat, Fibrillar structure of Nafion: Matching Fourier and real space studies of

corresponding films and solutions, *Macromolecules*, 2004, **37**(20), 7772–7783.
37 S. T. Cui, *et al.*, A molecular dynamics study of a nafion polyelectrolyte membrane and the aqueous phase structure for proton transport, *J. Phys. Chem. B*, 2007, **111**(9), 2208–2218.
38 M. H. Kim, *et al.*, SANS study of the effects of water vapor sorption on the nanoscale structure of perfluorinated sulfonic acid (NAFION) membranes, *Macromolecules*, 2006, **39**(14), 4775–4787.
39 W. Kubo, *et al.*, Imaging of Ionic Channels in Proton Exchange Membranes by the Nickel Replica Method, *J. Phys. Chem. C*, 2010, **114**(5), 2370–2374.
40 K. Schmidt-Rohr and Q. Chen, Parallel cylindrical water nanochannels in Nafion fuel-cell membranes, *Nat. Mater.*, 2008, **7**(1), 75–83.
41 S. A. Eastman, *et al.*, Effect of Confinement on Structure, Water Solubility, and Water Transport in Nafion Thin Films, *Macromolecules*, 2012, **45**(19), 7920–7930.
42 K. Valle, *et al.*, Hierarchically structured transparent hybrid membranes by in situ growth of mesostructured organosilica in host polymer, *Nat. Mater.*, 2006, **5**(2), 107–111.
43 K. L. More, R. Borup and K. S. Reeves, Identifying contributing degradation phenomena in PEM fuel cell membrane electrode assemblies *via* electron microscopy, *ECS Trans.*, 2006, **3**(1), 717–733.
44 G. C. Abuin, M. C. Fuertes and H. R. Corti, Substrate effect on the swelling and water sorption of Nafion nanomembranes, *J. Membr. Sci.*, 2013, **428**, 507–515.
45 P. A. Kienzle, J. A. Krycka and N. Patel, *Refl1D: Interactive depth profile modeler*, available from http://www.reflectometry.org/danse/software.
46 S. H. Anastasiadis, *et al.*, Neutron Reflectivity Studies Of The Surface-induced Ordering Of Diblock Copolymer Films, *Phys. Rev. Lett.*, 1989, **62**(16), 1852–1855.
47 R. E. Kass and A. E. Raftery, Bayes Factors, *J. Am. Stat. Assoc.*, 1995, **90**(430), 773–795.
48 C. F. Majkrzak, *et al.*, When beauty is only skin deep; optimizing the sensitivity of specular neutron reflectivity for probing structure beneath the surface of thin films, *J. Appl.Phys.*, 2011, **110**(10), 14.
49 K. W. Feindel, S. H. Bergens and R. E. Wasylishen, Use of hydrogen-deuterium exchange for contrast in (1)H NMR microscopy investigations of an operating PEM fuel cell, *J. Power Sources*, 2007, **173**(1), 86–95.
50 K. K. Pushpa, D. Nandan and R. M. Iyer, Hydrogen Isotope Effects In The Absorption Of Water By Perfluorosulfonate (Nafion-117) And Polystyrene Divinylbenzene Sulfonate (Dowex 50W) Ion-exchange Resins, *J. Chem. Soc., Faraday Trans.*, 1990, **86**(2), 409–412.
51 M. N. Tsampas, *et al.*, The effect of membrane thickness on the conductivity of Nafion, *Electrochim. Acta*, 2006, **51**(13), 2743–2755.
52 S. K. Dishari and M. A. Hickner, Confinement and Proton Transfer in Nafion Thin Films, *Macromolecules*, 2013, **46**(2), 413–421.
53 D. D. Borges, *et al.*, Inhomogeneous Transport in Model Hydrated Polymer Electrolyte Supported Ultrathin Films, *ACS Nano*, 2013, **7**(8), 6767–6773.
54 I. Kendrick, *et al.*, Elucidating the Ionomer-Electrified Metal Interface, *J. Am. Chem. Soc.*, 2010, **132**(49), 17611–17616.
55 W. L. Wu, *et al.*, Water Adsorption at a polyimide/silicon wafer interface, *Polym. Eng. Sci.*, 1995, **35**, 1000–1004.
56 B. D. Vogt, *et al.*, Interfacial Effects on Moisture Absorption in Thin Polymer Films, *Langmuir*, 2004, **20**, 5285–5290.
57 S. Kim, *et al.*, Surface-Induced Nanostructure and Water Transport of Thin Proton-Conducting Polymer Films, *Macromolecules*, 2013, **46**(14), 5630–5637.
58 P. W. Majsztrik, *et al.*, Water sorption, desorption and transport in Nafion membranes, *J. Membr. Sci.*, 2007, **301**(1–2), 93–106.
59 A. Z. Weber and J. Newman, Transport in polymer-electrolyte membranes – I. Physical model, *J. Electrochem. Soc.*, 2003, **150**(7), A1008–A1015.
60 J. A. Elliott and S. J. Paddison, Modelling of morphology and proton transport in PFSA membranes, *Phys. Chem. Chem. Phys.*, 2007, **9**(21), 2602–2618.
61 S. J. Paddison and T. A. Zawodzinski, Molecular modeling of the pendant chain in Nafion (R), *Solid State Ionics*, 1998, **113**, 333–340.
62 K. A. Mauritz and R. B. Moore, State of understanding of Nafion, *Chem. Rev.*, 2004, **104**(10), 4535–4585.
63 J. A. Dura, *et al.*, AND/R: Advanced neutron diffractometer/reflectometer for investigation of thin films and multilayers for the life sciences, *Rev. Sci. Instrum.*, 2006, **77**(7), 074301.
64 O. S. Heavens, *Optical properties of thin solid films*, Dover Publ., New York, 1991.
65 L. Nevot and P. Croce, Caracterisation des surfaces par reflexion rasante de rayons X. Applicaation a letude du polissage de quelques verres silicates, *Rev. Phys. Appl.*, 1980, **15**, 761–779.
66 J. A. Vrugt, *et al.*, Accelerating Markov Chain Monte Carlo Simulation by Differential Evolution with Self-Adaptive Randomized Subspace Sampling, *Int. J. Nonlinear Sci. Numer. Simul.*, 2009, **10**(3), 273–290.
67 G. Schwarz, Estimating Dimension Of A Model, *Ann. Stat.*, 1978, **6**(2), 461–464.
68 M. Bogdan, J. K. Ghosh and R. W. Doerge, Modifying the Schwarz Bayesian information criterion to locate multiple interacting quantitative trait loci, *Genetics*, 2004, **167**(2), 989–999.
69 K. W. Broman and T. P. Speed, A model selection approach for the identification of quantitative trait loci in experimental crosses, *J. Roy. Stat. Soc. B Stat. Meth.*, 2002, **64**(4), 641–656.